

## Dual-Polarization Observations of Microbursts Associated with Intense Convection: The 20 July Storm during the MIST Project

ROGER M. WAKIMOTO

*Department of Atmospheric Sciences, University of California, Los Angeles, California*

V. N. BRINGI

*Department of Electrical Engineering, Colorado State University, Fort Collins, Colorado*

(Manuscript received 9 October 1987, in final form 18 December 1987)

### ABSTRACT

A detailed case study of the microburst-producing storm on 20 July 1986 during the MIST Project is presented, together with visual (based on cloud photogrammetry) and radar observations during the life cycle of the storm. In particular, multiparameter radar information is seen to have important implications for operational detection of this wind shear event. Noteworthy is the observation of a small shaft (less than 1 km in horizontal dimensions) of near zero differential reflectivity ( $Z_{DR}$ ) surrounded by large positive  $Z_{DR}$  values in the main precipitation core within a microburst-producing downdraft. This " $Z_{DR}$ -Hole" implies a strong localized downdraft composed of melting hail.

### 1. Introduction

In recent years a class of violent thunderstorm outflows, called "microbursts" have received a great deal of attention owing to their devastating effect on aircraft performance (Fujita and Caracena 1977; NTSB 1983; Fujita 1985, 1986). Although an  $\sim 22 \text{ m s}^{-1}$  headwind-tailwind differential as reported by Fujita (1986) was instrumental in the Pan American airline crash at Kenner, Louisiana in 1982, Fujita and Wakimoto (1981a) have reported that some microbursts could produce tornado-force damage up to F3 intensity (Fujita 1981). In addition, Fujita (1985) has shown that a microburst striking Andrews Air Force Base a few minutes after Air Force One landed produced a total differential wind speed across the microburst center of greater than  $110 \text{ m s}^{-1}$ .

In studying wind shear events, scientists are confronted by two different problems:

- 1) to understand the differences between convective storms that produce microbursts from storms that are only accompanied by rain and relatively weak outflow.
- 2) to use current technology, by identifying signatures or precursors in order to establish criteria to nowcast<sup>1</sup> microbursts.

This paper deals with the latter issue.

<sup>1</sup> A nowcast is defined as a short period forecast of 0–30 minutes.

*Corresponding author address:* Roger Wakimoto, Dept. of Atmospheric Sciences, University of California, Los Angeles, CA 90024.

In an attempt to solve problem 2, meteorologists are faced with the difficult task of determining precursors before the microbursts strike the ground so that the information can be relayed to air traffic controllers who in turn provide advisory warning products to pilots. The three main tools for operationally detecting microbursts have been densely distributed surface weather stations, satellite imagery and, most importantly, Doppler radar (Wilson et al. 1984; Fujita 1985; Campbell 1986; McCarthy et al. 1986; Roberts and Wilson 1986, 1987; Eilts 1987).

During the spring and summer of 1986, the MIST (Microburst and Severe Thunderstorm) Project was operated near Huntsville, Alabama, to determine the three-dimensional structure of microbursts from thunderstorms in a wet (humid) region of the United States (Dodge et al. 1986). The project was timely since the two most recent microburst-related aircraft accidents at New Orleans in 1982 (NTSB 1983) and at Dallas in 1985 (Fujita 1986) appeared to be caused by the type of storm that might be encountered in the Alabama area. On 20 July 1986, perhaps the most comprehensive dataset on a microburst and its parent thunderstorm was collected. Surface damage from the microburst winds was located by ground and aerial survey and estimated to have occurred at  $\sim 1324$  CST with surface divergence first detected at  $\sim 1321$  CST.

A description of the MIST Project is presented in section 2. Surface and upper-air data used to describe the synoptic environment are presented in section 3. Section 4 examines the 20 July microburst and parent storm with the use of satellite imagery and Doppler

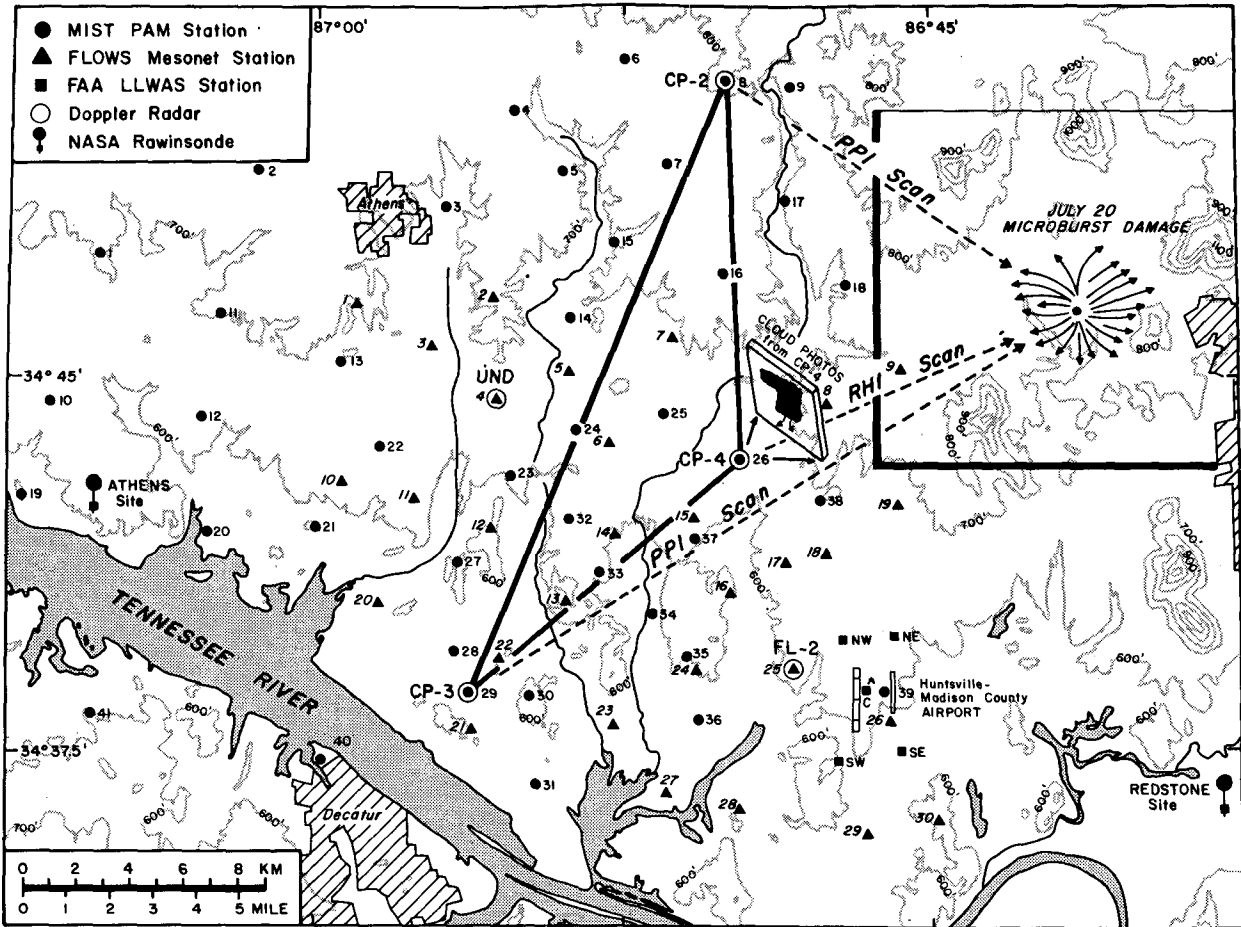


FIG. 1. The MIST/FLOWS network in Alabama. The surface damage caused by the 20 July storm is shown. The CP-2 and CP-3 radars scanned the region in a Plan-Position Indicator (PPI) mode while the CP-4 radar collected data in a Range-Height Indicator (RHI) mode. Photos of the parent thunderstorm were taken from the CP-4 site. Rawinsondes were launched from the Redstone site. The boxed-in area is enlarged in Fig. 6.

radar information. Application of the dual-polarization, differential reflectivity ( $Z_{DR}$ ) radar measurement to detect storm microphysical evolution and subsequent microburst development is emphasized. A summary and discussion of the results is presented in section 5.

## 2. The MIST project

There have been two previous field studies that have examined the microburst phenomenon: the NIMROD (Northern Illinois Meteorological Research On Downbursts) and JAWS (Joint Airport Weather Studies) Projects near the Chicago and Denver areas, respectively. During the NIMROD Project in 1978 (Fujita 1979), single-Doppler data on several microbursts were collected for the first time. Unfortunately, the large base lines between radars ( $\sim 60$  km) did not allow for any multi-Doppler reconstruction of thunderstorm

flow fields, which became one of the key scientific objectives of the JAWS Project in 1982 (McCarthy et al. 1982).

Based on surface mesonet data, it has been shown that 155 of the 186 microbursts (83%) within the JAWS network were dry, i.e., a microburst that is accompanied by little or no rain (Wakimoto 1985). (This figure may be misleading in that rainfall could have fallen near the downdraft center in some cases but not at a recording surface station.) The observation that severe microburst wind shears may be associated with virga shafts from innocuous-looking clouds with reflectivities as low as 10 dBZ at 500 m AGL (Kessinger et al. 1986; Roberts and Wilson 1986) may have been the most important finding from JAWS. Examples of this type of microburst are shown in Fujita (1985), and McCarthy and Serafin (1984, p. 120). In the latter case, the peak wind speed was  $23.5 \text{ m s}^{-1}$  and no rain was detected at the surface. Dry microbursts are prevalent over the High Plains owing to the deep dry layers (av-

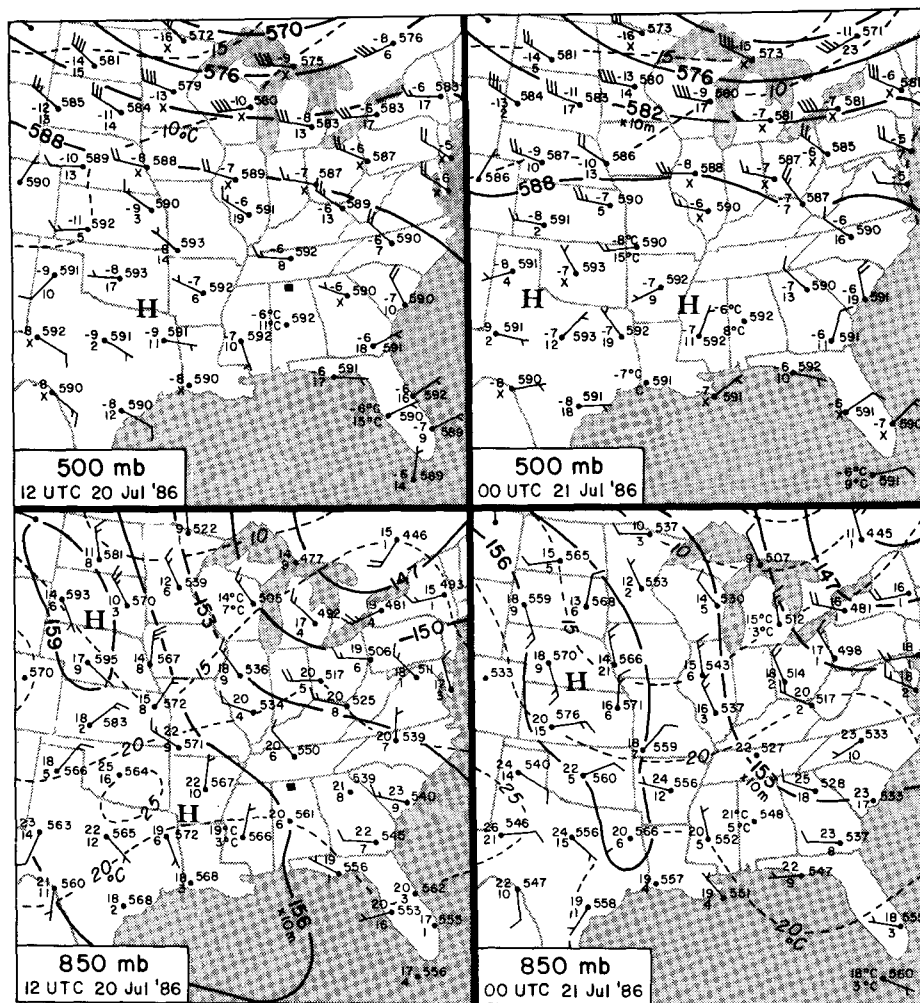


FIG. 2. The 500 and 850 mb analyses for 1200 UTC 20 July and 0000 UTC 21 July. Black lines are contours and dashed lines are isotherms. Temperature, dewpoint depression, and height are plotted. One flag, full barb, and half barb denote  $25 \text{ m s}^{-1}$ ,  $5 \text{ m s}^{-1}$ , and  $2.5 \text{ m s}^{-1}$ , respectively. The small black box in northern Alabama on the upper-level charts at 1200 UTC 20 July covers the same area as Fig. 1.

erage cloud base  $\sim 500$  mb) and insolation that frequently produces a dry-adiabatic subcloud layer. Several investigators have shown that with this type of boundary layer, evaporative cooling is the primary forcing mechanism for strong downdrafts even when accompanied by little precipitation (Brown et al. 1982; Caracena et al. 1983; Kamburova and Ludlam 1966; Krumm 1954; Wakimoto 1985; Srivastava 1985). However, in the southeast area of the United States where there is a relatively shallow subcloud (and therefore dry-adiabatic) layer, evaporative cooling may not be the only mechanism driving the downdraft. In addition, Srivastava (1985) has shown that microphysical considerations are crucial in any downdraft calculation; therefore, there will be important differences between the cold cloud bases of storms over the High Plains and the warm-based clouds over the southeast.

The foregoing considerations led to the organization and operation of the MIST Project. MIST was only one part of a much larger project entitled the Cooperative Huntsville Meteorological Experiment (COHMEX). The Federal Aviation Administration (FAA) component of COHMEX called FLOWS (FAA-Lincoln Laboratories Operational Weather Studies) was concerned with the development and testing of automatic algorithms for wind shear detection using Doppler radar. The combined MIST/FLOWS network is shown in Fig. 1. Readers interested in the description of other observing platforms during COHMEX are referred to Dodge et al. (1986).

There were five Doppler radars deployed during the project: the three NCAR (National Center for Atmospheric Research) Doppler radars (CP-2, CP-3, and CP-4) in support of MIST; and the FL-2 (Evans and John-

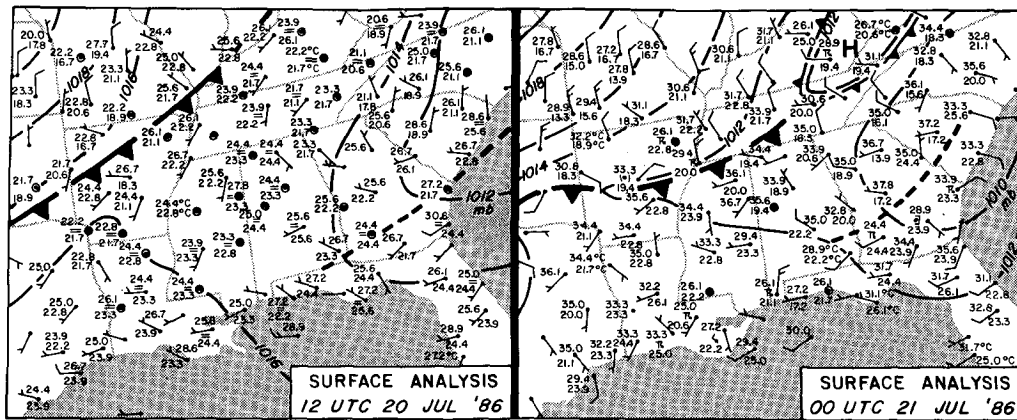


FIG. 3. Surface analyses for 1200 UTC 20 July and 0000 UTC 21 July 1986. Black lines are isobars. Temperature and dewpoint temperature are plotted. One full barb and half barb denote  $5 \text{ m s}^{-1}$  and  $2.5 \text{ m s}^{-1}$ , respectively.

son 1984) and University of North Dakota (UND) Doppler radars in support of FLOWS. Located throughout the network were 41 NCAR PAM (Portable Automated Mesonet) stations and 30 FLOWS mesonet stations (Wolfson 1987) recording air temperature, dewpoint temperature, pressure, wind speed and direction, and rainfall data. In addition, there were 5 stations that comprise the FAA Low-Level Wind Shear Alert System (LLWSAS) surrounding the Huntsville–Madison County Airport. Two of the National Aeronautics and Space Administration (NASA) sponsored rawinsonde sites (Redstone and Athens) are also shown in Fig. 1.

3. Synoptic environment

Charts at the 500 and 850 mb levels for 1200 UTC 20 July and 0000 UTC 21 July are shown in Fig. 2. A strong ridge built over the southern states at the 500 mb level with an axis oriented approximately east–west from central Texas through Georgia. There are no obvious short-wave troughs entering the Alabama area on these two charts. At the 700 mb (not shown) and the 850 mb levels, a distinct trough oriented northeast to southwest is apparent through Michigan, Indiana, Illinois, and Missouri at 1200 UTC 20 July and Ohio, Kentucky, and Tennessee at 0000 UTC 21 July. Weak cold air advection is noted west of the trough axis. The small black box in northern Alabama shown at 1200 UTC represents the MIST area (see in Fig. 1).

A cold front at the surface (Fig. 3) is associated with the short-wave trough at the upper levels. Recall that the microburst occurred at 1324 CST (1921 UTC) on 20 July. Accordingly, the storm developed in the warm sector ahead of the cold front. This prefrontal air mass was moisture laden as shown by the fog reported throughout the area at 1200 UTC. In the late afternoon and evening at 0000 UTC a surface mesohigh formed over northern Tennessee, Kentucky, and West Virginia

as a result of vigorous thunderstorm activity along the cold front. Also apparent in Fig. 3 is a trough over South Carolina and Georgia which appears to be supported at the 850 mb level (Fig. 2). Scattered showers and thunderstorms are reported ahead (southeast) of this trough at 0000 UTC.

The sounding at 1200 CST (~90 min. before the microburst) from the Redstone site located  $\approx 19 \text{ km}$  south southeast of the center of the microburst damage is shown in Fig. 4. The observed cloud base on the figure was based on a photogrammetric analysis of cloud pictures and agrees with the convective condensation level.

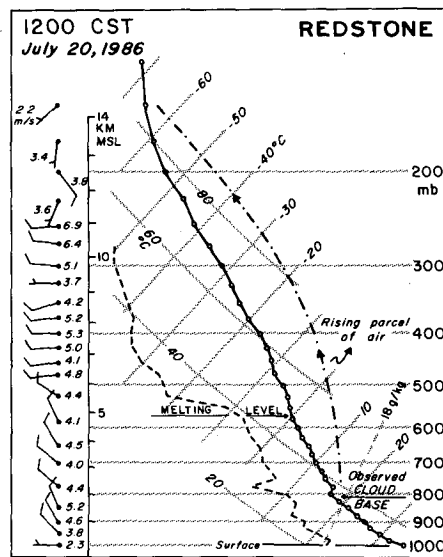


FIG. 4. Sounding from the Redstone site approximately one hour before the 20 July storm formed (see Fig. 1 for locations). The black line and dashed line are the temperature and dewpoint temperature curves, respectively. The dash-dot line represents the wet-bulb potential temperature of a rising parcel. The melting level and observed cloud base (based on cloud photogrammetry) are also indicated.

TABLE 1. Comparison of typical dry microburst and 20 July storm soundings.

	Dry microburst sounding	20 July storm sounding
Subcloud lapse rate	Dry adiabatic	Near dry adiabatic
Subcloud layer depth	3.5 km	2 km
Subcloud Layer mixing ratio	Constant (3–5 g kg <sup>-1</sup> )	Not constant (~14 g kg <sup>-1</sup> )
Lifted index	Neutral	~ -7

At this time it may be useful to compare the sounding in Fig. 4 with the model of the dry microburst sounding developed by Wakimoto (1985) (Table 1). The shallower subcloud layer on 20 July is not as favorable for evaporative cooling to produce a strong downdraft; however, the relatively moist subcloud layer may promote large negative vertical velocities based on the results from Srivastava (1985). He has shown that, without entrainment, high relative humidity results in stronger downdrafts since a descending parcel is virtually cooler than the environment because it is drier.

Figure 4 is similar to one shown by Eilts and Doviak (1987) for an Oklahoma downburst from an intense thunderstorm where a moist subcloud layer is topped by a layer of dry air (the same feature is observed in Fig. 4 at ~790 mb). The sounding at Redstone also has a significant dry layer above ~570 mb resulting in potentially cool air conducive to strong downdrafts (Caracena and Maier 1987). Clearly, a detailed study similar to the one performed by Wakimoto (1985) needs to be undertaken to understand the forecast criteria for wet microbursts in this region of the country.

#### 4. Satellite and radar observations of the 20 July storm

##### a. Satellite imagery

During the field operations of MIST, the NCAR Doppler radars performed coordinated sector scans starting at ~1242 CST over the area where the 20 July storm developed, well before any significant radar echo was apparent. This action was prompted by the observation of a weak convergence line in the single-Doppler velocity field, a situation often conducive to convection initiation (Wilson and Schreiber 1986). Satellite imagery presented in Fig. 5 adds some insight as to the possible origin of this convergence line.

The dominant cloud feature over Tennessee, Mississippi, Alabama, and western Georgia are the "cumulus cloud lines" (Anderson et al. 1972) oriented northwest-to-southeast. Caution must be exercised when using these lines to define the low-level winds. The surface analysis at 1800 UTC (not shown) and 0000 UTC 20 July (Fig. 3) only exhibit a tendency for northwesterly flow based on the surface wind reports,

a fact also confirmed by the Redstone sounding (Fig. 4), recording a westerly wind at the surface at 1200 CST (1800 UTC). However, at slightly higher levels between the 850 and 700 mb levels, there was a persistent flow from the northwest along which these cumulus clouds were aligning. Recall that cloud base over Northern Alabama was ~800 mb (Fig. 4). The recognition of this pattern is important since the 20 July storm was one of many storms initiated along these cloud lines over the southeast United States.

The enhanced cumulus activity along one of the cumulus lines is shown in Fig. 5(b) by the black arrow. Recall that the image time is for the beginning of the scan near 89°N latitude; therefore, the data over northern Alabama is valid for ~1905 UTC (1305 CST). These corrected times will be useful when comparing with the radar analyses in section 4b. The storm is well-developed by 1914 UTC (Fig. 5c) with the beginning stages of an anvil apparent, which is clearly visible by 1930 UTC (Fig. 5d). The microburst struck the surface between these two image times. The images at 2000 and 2030 UTC show the dissipation of the storm with only the faint remnants of the anvil along the northern Alabama border in Fig. 5f.

When viewing the satellite images in Fig. 5, it is striking that the microburst-producing storm over the MIST network is not ominous in appearance, especially when compared to other convective activity to the southeast near the Alabama–Georgia border. This observation suggests that satellite imagery may not be able to identify storms producing severe wind shears as first proposed by Fujita (1978) and Fujita and Wakimoto (1981a). This supports more recent results from Wakimoto (1983) and Fujita (1986), documenting cases where visual and infrared satellite imagery did not reveal an obvious signature conducive to microburst activity.

##### b. Radar observations

The 20 July storm formed in the eastern part of the MIST network as shown in Fig. 1. Streamlines of tree and crop damage at the surface are shown on this figure. All three NCAR radars performed coordinated sector scans on the storm; CP-2 and CP-3 in a plan-position indicator (PPI) mode and the CP-4 radar in a range-height indicator (RHI) mode. Photos of the thunderstorm using a 35 mm camera were also taken by Kevin Knupp at the CP-4 site. Unfortunately, the UND and FL-2 radars were not operational on this day.

An enlargement of the box shown in Fig. 1 is shown in Fig. 6 which presents a time series of the PPI scans from the CP-2 radar. The microburst impacted the surface at ~1321 CST based on low-level Doppler velocities and is shown by the black arrows at 1320:53 CST in Fig. 6 representing the direction of tree fall and vegetation damage. The FLOWS mesonet station indicates a slight shift in wind direction from the north-

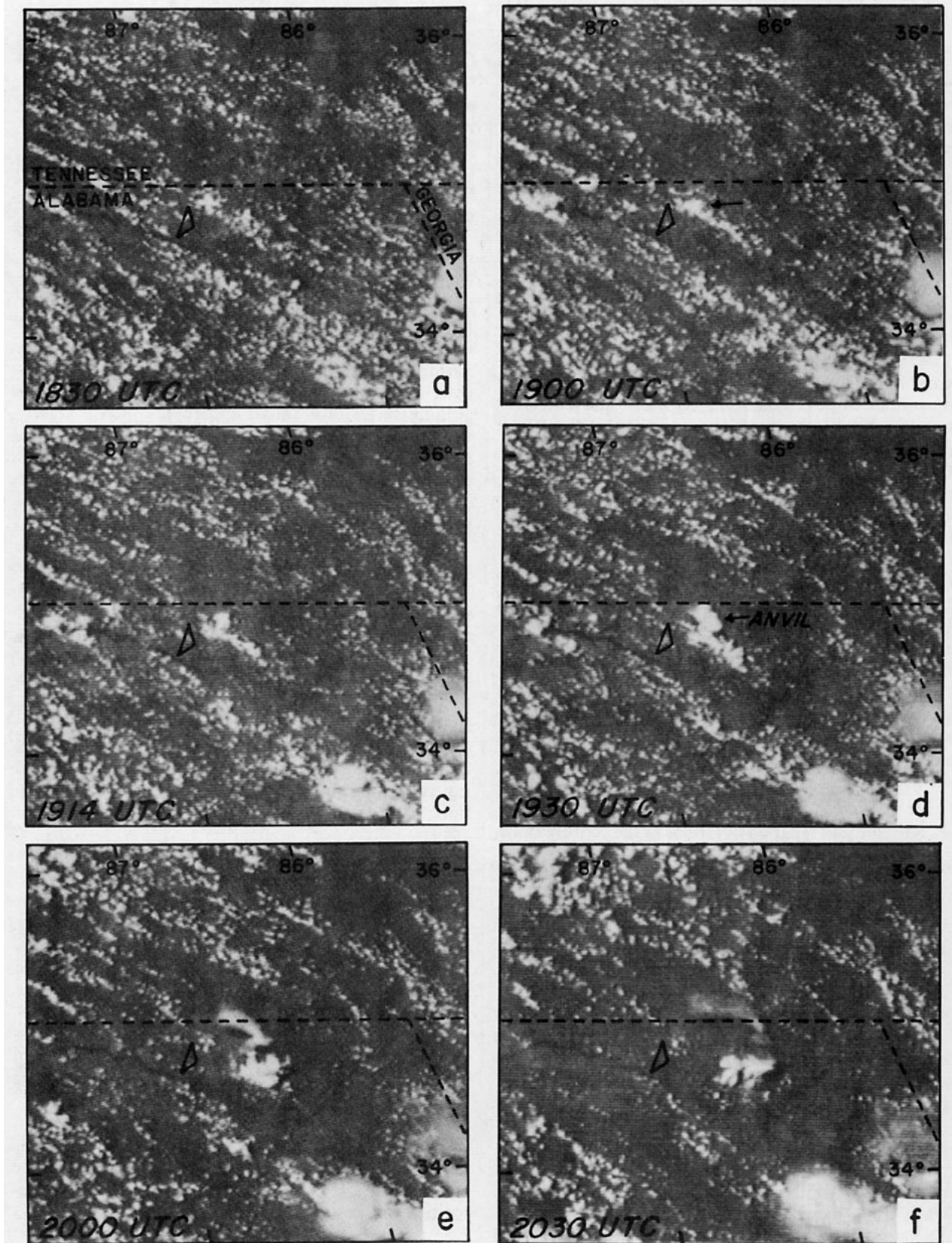


FIG. 5. Visual satellite imagery over the MIST network for 1830, 1900, 1914, 1930, 2000 and 2030 UTC 20 July 1986. The black triangle denotes the location of the NCAR Doppler radars shown in Fig. 1.

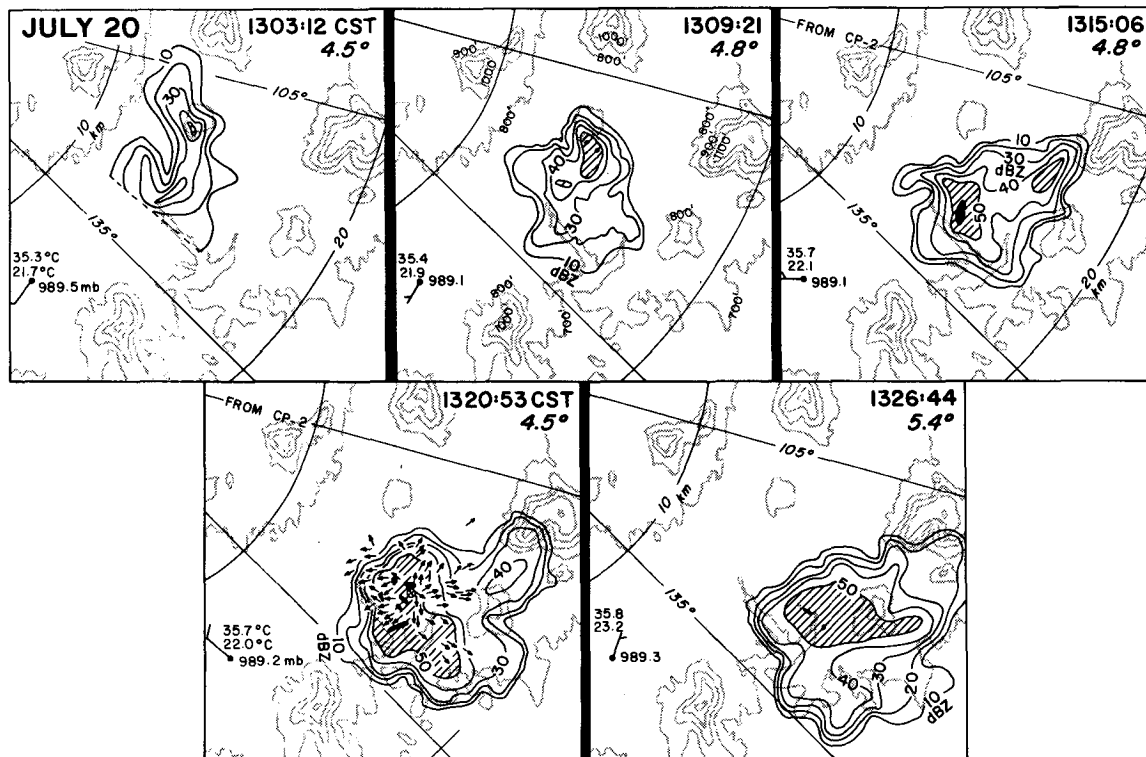


FIG. 6. Time series of PPI sector scans from the CP-2 radar for the 20 July storm. Black arrows at 1320:53 CST represent direction of tree fall and vegetation damage caused by the microburst, based on a survey by Greg Forbes. Temperature, dewpoint temperature, wind speed and direction, and station pressure from FLOWS mesonet station 9 are shown. One barb and half barb denote 5 and 2.5  $\text{m s}^{-1}$ , respectively. Gray lines are topography.

northeast at 1326:44 CST as the outflow from the storm expands. As shown by the topography in the figure, the microburst occurred in a depressed geographic region surrounded by small hills.

From the position of the storm in Fig. 1, it is evident that excellent multi-Doppler radar data exists to reconstruct the three-dimensional kinematic wind field of the 20 July storm. Although this is currently being accomplished and will be presented in a future article, this paper is primarily concerned with operational aspects of the storm with recent technology for now-casting microbursts. Accordingly, only single-Doppler analysis and dual-polarization data are shown in this section.

#### 1) CLOUD PHOTOGRAMMETRY AND RADAR DATA FROM CP-4

It was recognized early in the planning stages of MIST that cloud photography would play an important role in studying microburst-producing storms. Airline pilots who often rely on visual observations to navigate an aircraft would perhaps find this very enlightening. Although Doppler radar information is invaluable, pilots must know the appearance of these types of storms. Accordingly, cloud photography combined with radar

data from the CP-4 radar provides a unique view of the 20 July microburst storm.

An azimuth and elevation angle grid was superimposed on each cloud photo. Since the storm was  $\sim 14$  km from the CP-4 radar site, it can be assumed that this grid also corresponds to the azimuth and elevation angles from the radar antenna. For each radar volume scan the distance to the maximum reflectivity center of the storm was determined. At this range a cross section of radar reflectivities perpendicular to the radar beam axis was constructed and then superimposed on the cloud photo. The results of this photogrammetric combination of cloud pictures and radar data are shown in Fig. 7. The height grid on the cloud photos is based on the distance to the maximum reflectivity center and reveals a visual cloud base of  $\sim 1.8$  km AGL.

The first cloud picture at 1303:10 CST was taken before the CP-4 radar began collecting data (Fig. 7a). No convective tower was visible at this time. By 1307:13 CST (Fig. 7b), a distinct growing tower developed reaching a height between 8–9 km AGL. The radar reflectivities are surprisingly high with two cores of over 60 dBZ. The edge of the cloud top corresponds to the 10 dBZ isopleth, an observation noted previously by Fujita et al. (1979). Even though the radar reflectivity factor exceeds 50 dBZ below cloud base, visual obser-

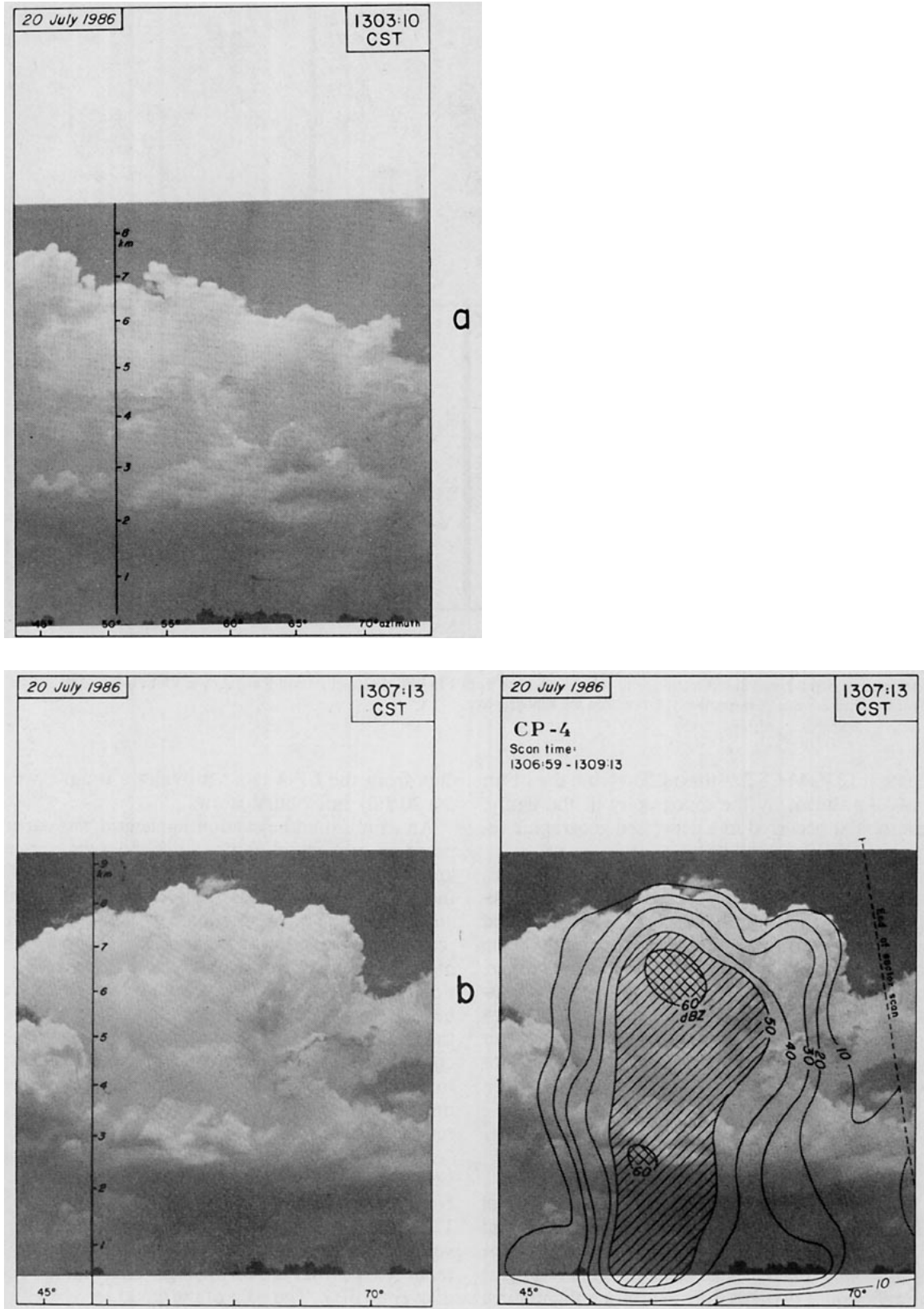


FIG. 7. Doppler radar data from CP-4 photogrammetrically combined with cloud photos for the 20 July storm. Photos taken by Kevin Knupp.

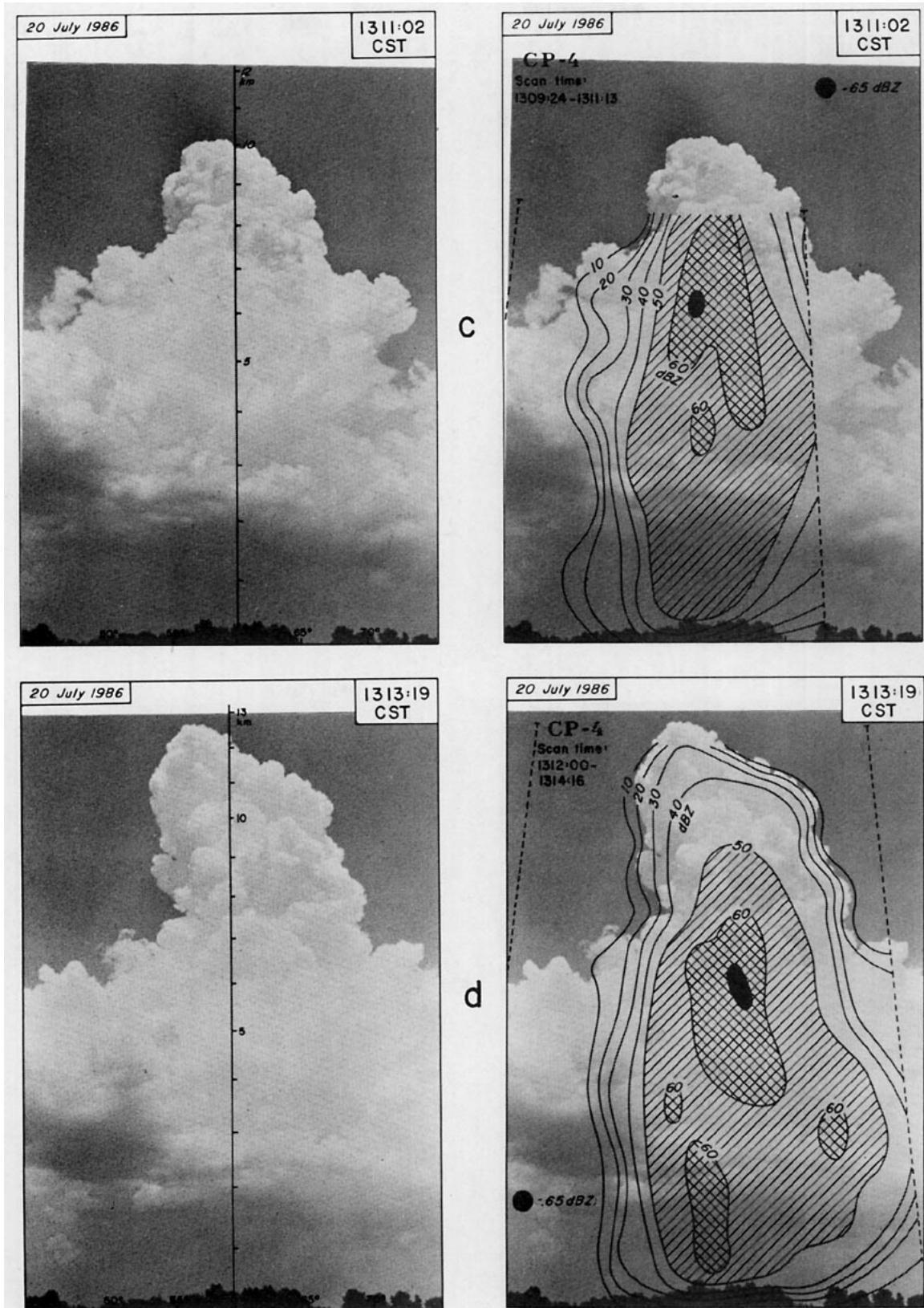


FIG. 7. (Continued)

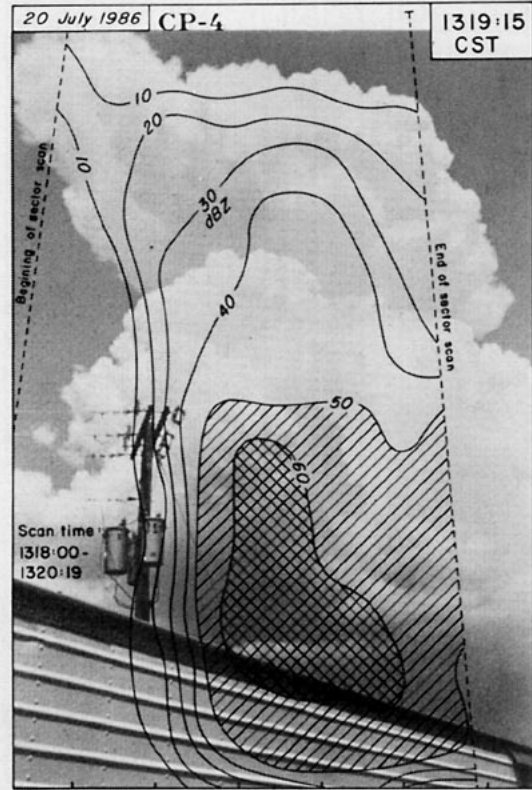
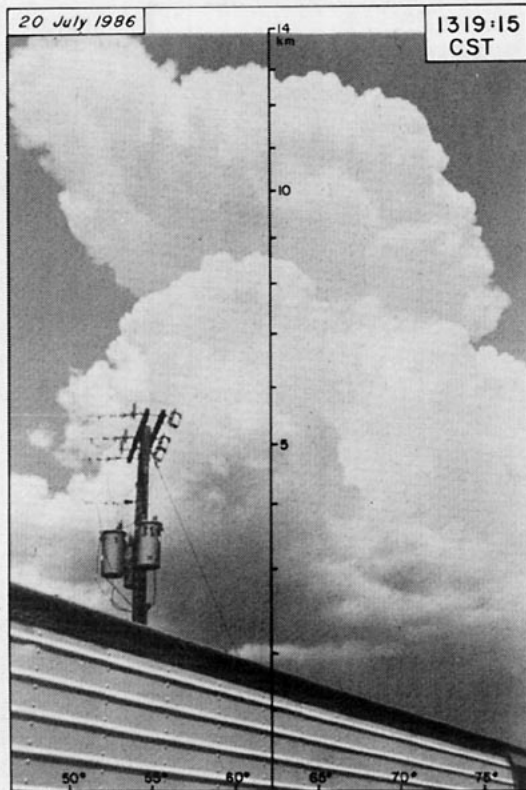
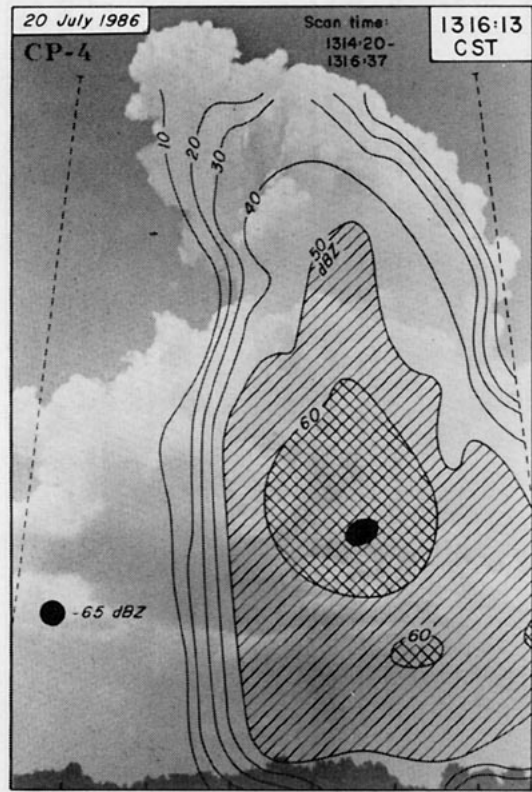
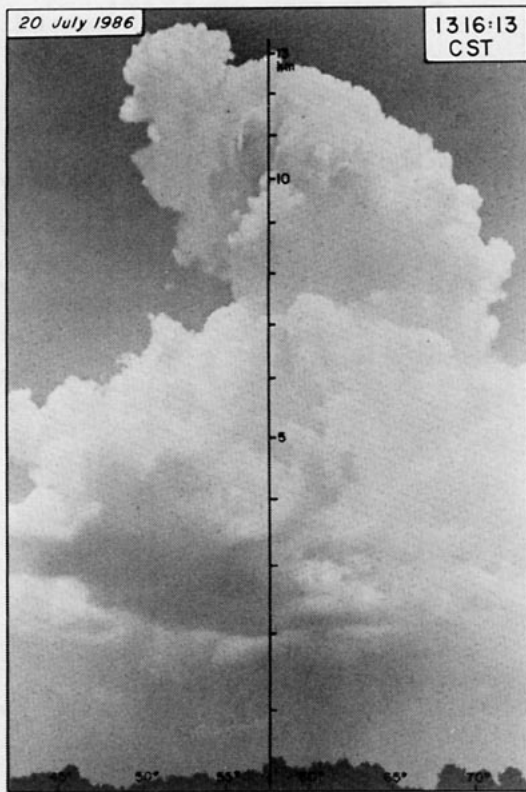


FIG. 7. (Continued)

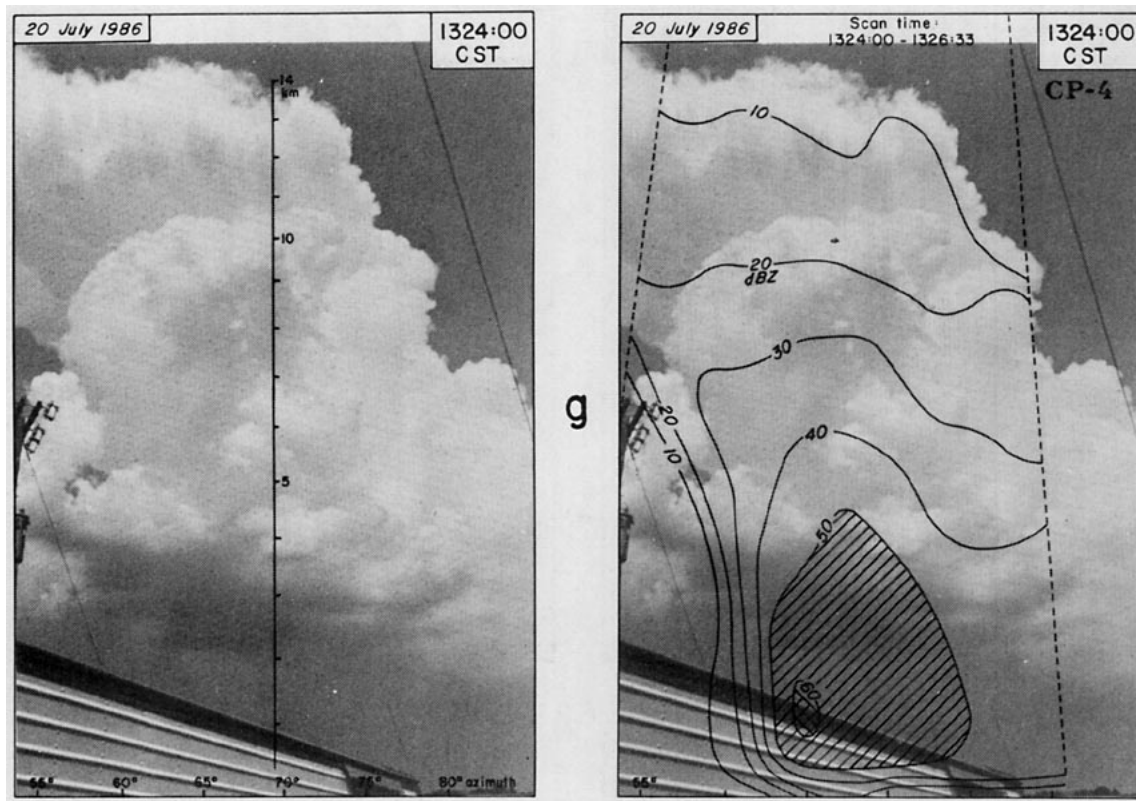


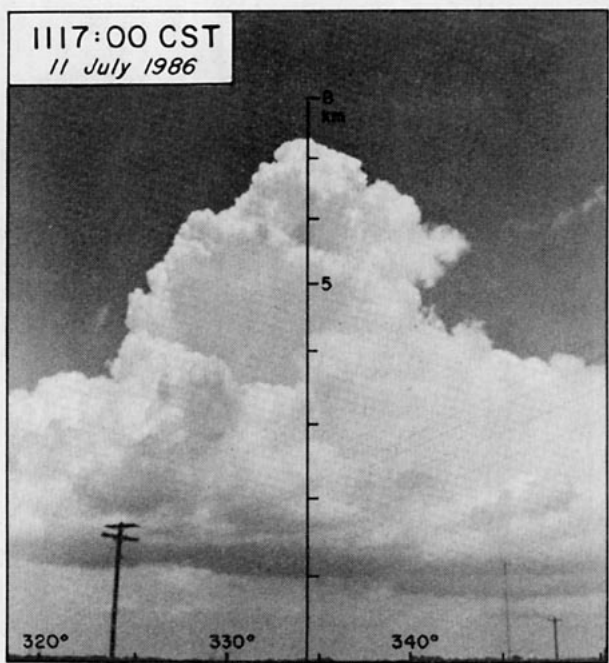
FIG. 7. (Continued)

vation at that time (and the original color pictures of Fig. 7) did not reveal an intense rainshaft. This is understandable since radar reflectivity alone is not a true indicator of the microphysics of storms. In the Rayleigh limit, the radar backscatter cross section of a drop is proportional to  $d^6$  (where  $d$  is the drop diameter); thus, it is well known that a large number of small drops can produce the same radar reflectivity as a small number of large drops. It is believed that the lack of an intense visual rainshaft yet high radar reflectivities below cloud base in Fig. 7b is a result of a low concentration of large raindrops, a hypothesis that is confirmed in the next section using the differential reflectivity ( $Z_{DR}$ ) measurement. It should be noted that the rapid decrease of radar reflectivities close to the surface in all of the figures is a result of "radar beam blockage" from trees that are visible on the horizon.

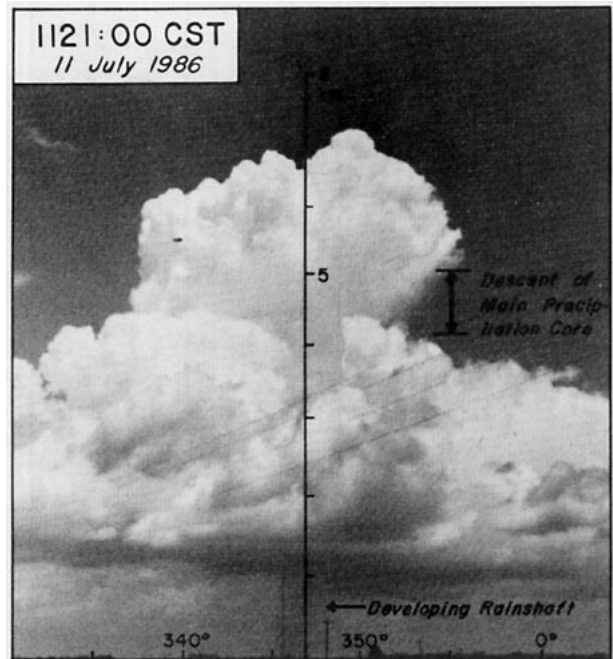
The storm continues to grow rapidly and by 1311:02 CST (Fig. 7c) and has reached a height of ~10 km AGL. Owing to this unexpected growth, the CP-4 radar did not scan to the top of the storm as shown in the figure. Radar reflectivities exceeding 60 dBZ were still being recorded at the highest elevation angle. A precipitation core of greater than 65 dBZ is located at ~6 km AGL. The first indication of an anvil is apparent at 1313:19 CST (Fig. 7d). The storm top is ~13 km, close to the equilibrium level determined from the Redstone sounding in Fig. 4. Although there are 4 cores

of radar reflectivities greater than 60 dBZ the main core containing the 65 dBZ core has begun its descent toward the surface. Based on  $Z_{DR}$  radar observations presented in the next section, it is believed that the other 3 cores of 60 dBZ are comprised of large drops while the main core is composed of ice particles. Although a single Doppler radar cannot directly measure downdrafts unless the antenna points vertically, the rapid descent of a precipitation core and the collapse of a storm are often indications of the initiation of a downdraft. This is not surprising since precipitation drag forces would be expected to be a maximum at the precipitation core.

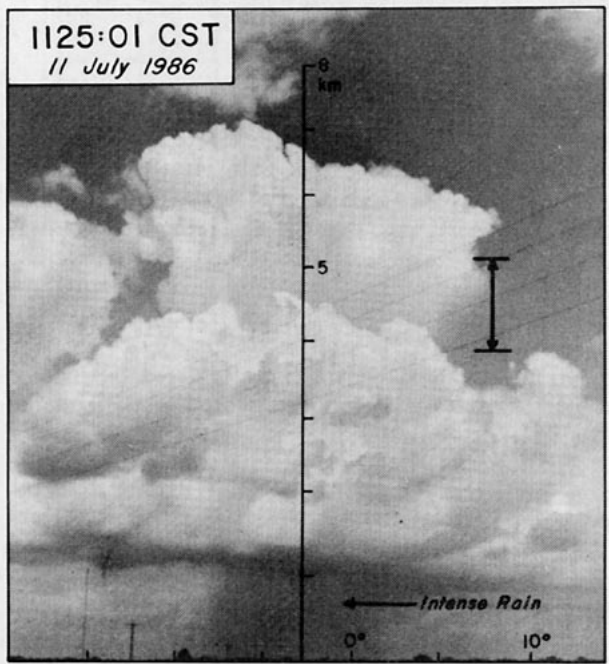
The descent of the main precipitation core continues at 1316:13 CST (Fig. 7e) and is close to cloud base at this time. Unfortunately, as this core descends below cloud base at 1319:15 CST (Fig. 7f), the top of a trailer is obscuring the foreground. The maximum radar reflectivity values have decreased below 65 dBZ. A decrease in reflectivity with decreasing height in a descending precipitation core is suggestive of evaporative cooling in a possible accelerating downdraft. However, it is also possible to have decreasing reflectivity owing to changes in precipitation type, particle size distribution and fall speeds. Besides the descent of the main precipitation core, another feature in Fig. 7 is the weakening of the vertical gradient of radar reflectivity factor near the cloud top. In Fig. 7b this gradient is



a



b



c

FIG. 8. Cloud photos of the 11 July storm from the CP-4 radar site. The descent of the main precipitation core is marked by a visual change on the sides of the convective tower to a laminar/glaciated appearance. An intense rainshaft is visible at the surface within minutes after this observation.

~25 dBZ km<sup>-1</sup> and reduces to ~10 dBZ km<sup>-1</sup> in Fig. 7f. In other thunderstorm cases observed during MIST, this change in the radar reflectivity factor gradient was almost always apparent, even when the descent of the main precipitation core was difficult to locate.

A few minutes after Fig. 7f (~1321 CST) the microburst struck the surface at an azimuth of ~67° from

CP-4. The collocation of the maximum reflectivity core with the microburst center has been previously documented by Roberts and Wilson (1986, 1987) using JAWS data. The microburst reached full intensity at 1324:00 CST (Fig. 7g) as the maximum radar reflectivity factor in the precipitation core decreased substantially. Maximum single Doppler velocity differ-

ential across the microburst center (i.e., in the direction in and out of the cloud photos shown in Fig. 7) observed by the CP-4 radar was  $\sim 30 \text{ m s}^{-1}$ . The anvil which first appeared glaciated at 1319:15 CST is now well developed.

Approximately 8 minutes passed after the 20 July storm reached its maximum visual height before the microburst winds appeared at the surface. It should also be mentioned that during the initial descent of the precipitation core the sides of the 20 July thunderstorm tower became laminar/glaciated in appearance. Unfortunately, this observation was not apparent from the CP-4 site owing to low-level clouds in the foreground, although it was observed from other locations in the network. However, this change in the visual structure on the sides of the main convective tower during the initial descent of the precipitation core was well documented for a storm on 11 July as shown in Fig. 8. In Fig. 8a the storm is still growing and no visible rainshaft is apparent beneath cloud base. It should be noted, however, that similar to the 20 July storm, the radar reflectivities (not shown) below cloud base exceeded 60 dBZ at this time. By 1121:00 CST (Fig. 8b) the initial descent of the precipitation core has begun and the sides of the convective tower between 4–5 km AGL appears to be laminar/glaciated in appearance. The first indication of a rainshaft has developed below cloud base although the radar reflectivities are still between 50–60 dBZ. With the onset of a very intense rainshaft at 1125:01 CST (Fig. 8c) this laminar/glaciated structure has expanded. This visual change in the structure of the middle section of a convective tower is important for airline pilots to recognize since it appears to be a signature of the initial descent of a precipitation core. Depending on the depth of the storm, an intense rainshaft can be expected to reach the surface within minutes after this visual observation.

There are two important points concerning this change in the visual structure and its implications for microburst warnings. First, each of the two examples shown in Figs. 7 and 8 is an "air mass" thunderstorm (Byers and Braham 1949), i.e., a thunderstorm evolving through three distinct stages (cumulus, mature, and dissipating) in a relatively short period of time. It is not clear that other storm types would exhibit this visual change. Second, although this laminar/glaciated appearance on the sides of a convective tower is an indication of the collapse of a thunderstorm it does not necessarily imply dangerous microburst wind shears at the surface. Only heavy rain and weak outflow were detected at the surface for the 11 July storm!

## 2) MULTIPARAMETER RADAR DATA

The limitations of using radar reflectivity measurements in determining the microphysics of storms was discussed earlier. Many of these limitations are re-

moved with the use of the NCAR CP-2 multiparameter radar. The term "multiparameter" refers to measurements made in addition to reflectivity and Doppler velocity. This radar combines differential reflectivity ( $Z_{DR}$ ), linear depolarization ratio (LDR), and dual-wavelength measurements (10 and 3 cm) for determining the microphysical characteristics of storms (Bringi et al. 1986a,b).

In this paper we focus on the differential reflectivity or  $Z_{DR}$  which was first postulated by Seliga and Bringi (1976) as a means of estimating the median drop sizes of exponentially distributed raindrop spectra. In rainfall,  $Z_{DR}$  is generally in the range 0–5 dB, the positive values being due to the nearly oblate shapes of the larger raindrops coupled with a high degree of alignment of their symmetry axis which is near vertical. Let the radar reflectivity factors at horizontal (vertical) polarizations be  $Z_H$  ( $Z_V$ ). Then, the measurement of  $Z_{DR}$  is shown schematically in Fig. 9. The figure insert shows  $Z_{DR}$  as a function of median raindrop size  $D_0$  for an exponential distribution of the form  $N(D) = N_0 \exp(-3.67D/D_0)$ . Since the oblateness of raindrops is a smoothly increasing function of raindrop size (Pruppacher and Klett 1978), the  $Z_{DR}$  measurement can be directly related to the mean axis ratio of the raindrops and, hence, to  $D_0$  (Bringi et al. 1986a; Hall et al. 1980). The insert of Fig. 9 also shows a spherical hailstone for which  $Z_{DR} = 0 \text{ dB}$ . While hailstones are generally nonspherical in shape, they tumble while falling resulting in  $Z_{DR} \sim 0 \text{ dB}$  or even slightly negative (Bringi et al. 1984, 1986b), while the corresponding reflectivity factor generally exceeds about 45 dBZ. This feature, which can be used to detect hailshafts penetrating below the melting level

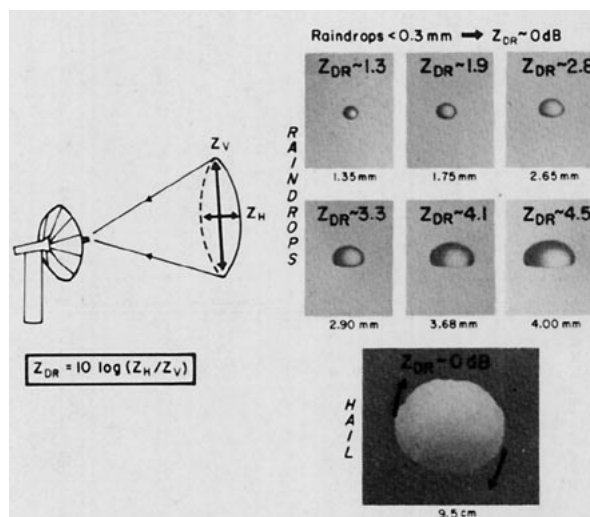


FIG. 9. Summary of typical  $Z_{DR}$  values for raindrops of various sizes and hail. These  $Z_{DR}$  values are based on the median volume diameter from Bringi et al. (1986a). The black arrows on the hail particle represent the tumbling motions as it moves in a thunderstorm. (Raindrop pictures courtesy of Cloud Physics Group at UCLA, hail picture courtesy of Nancy Knight at NCAR.)

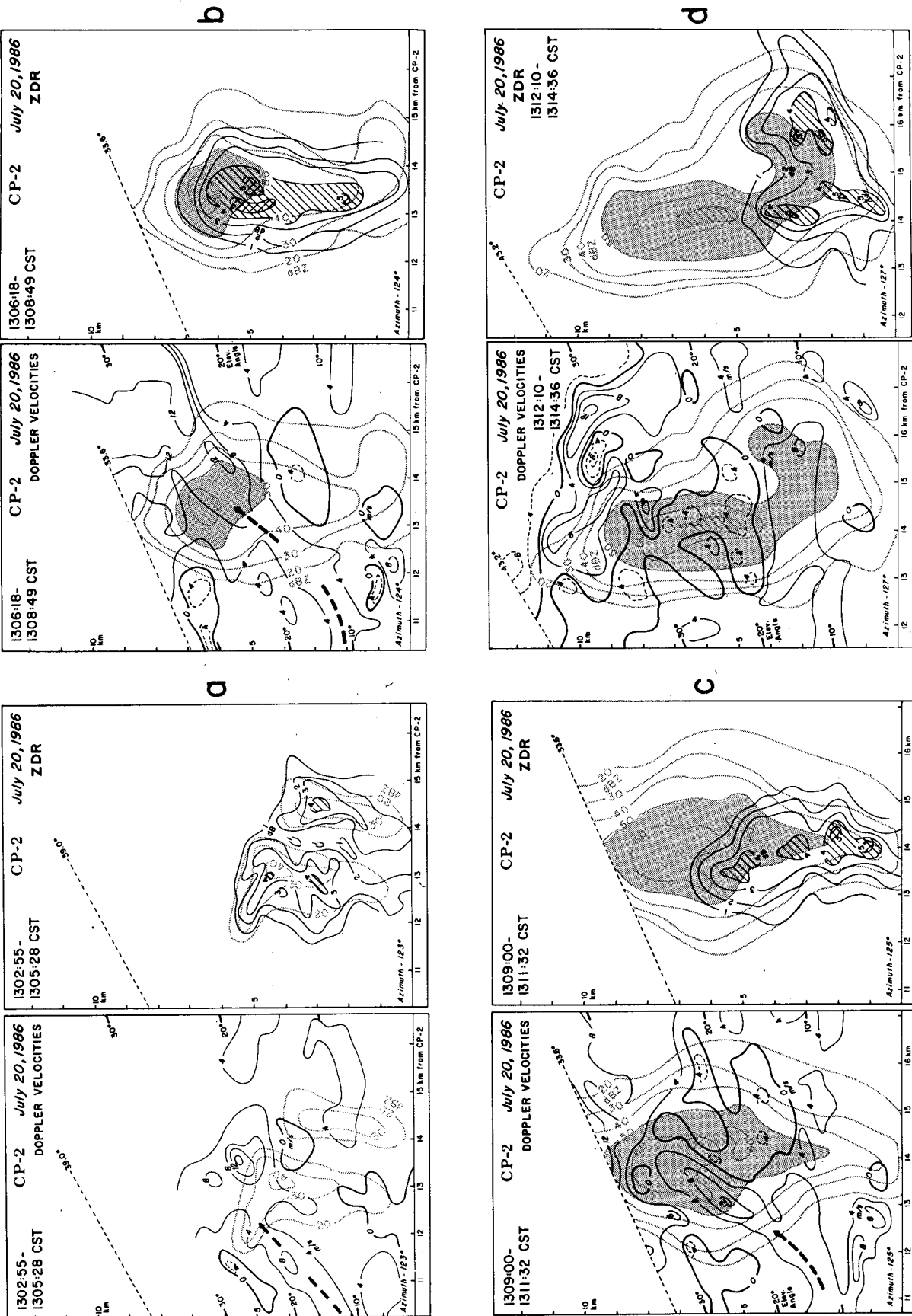


FIG. 10. The RHI cross sections of single Doppler velocities, radar reflectivities and Zdr from the CP-2 radar. Gray areas are radar reflectivities greater than 50 dBZ.

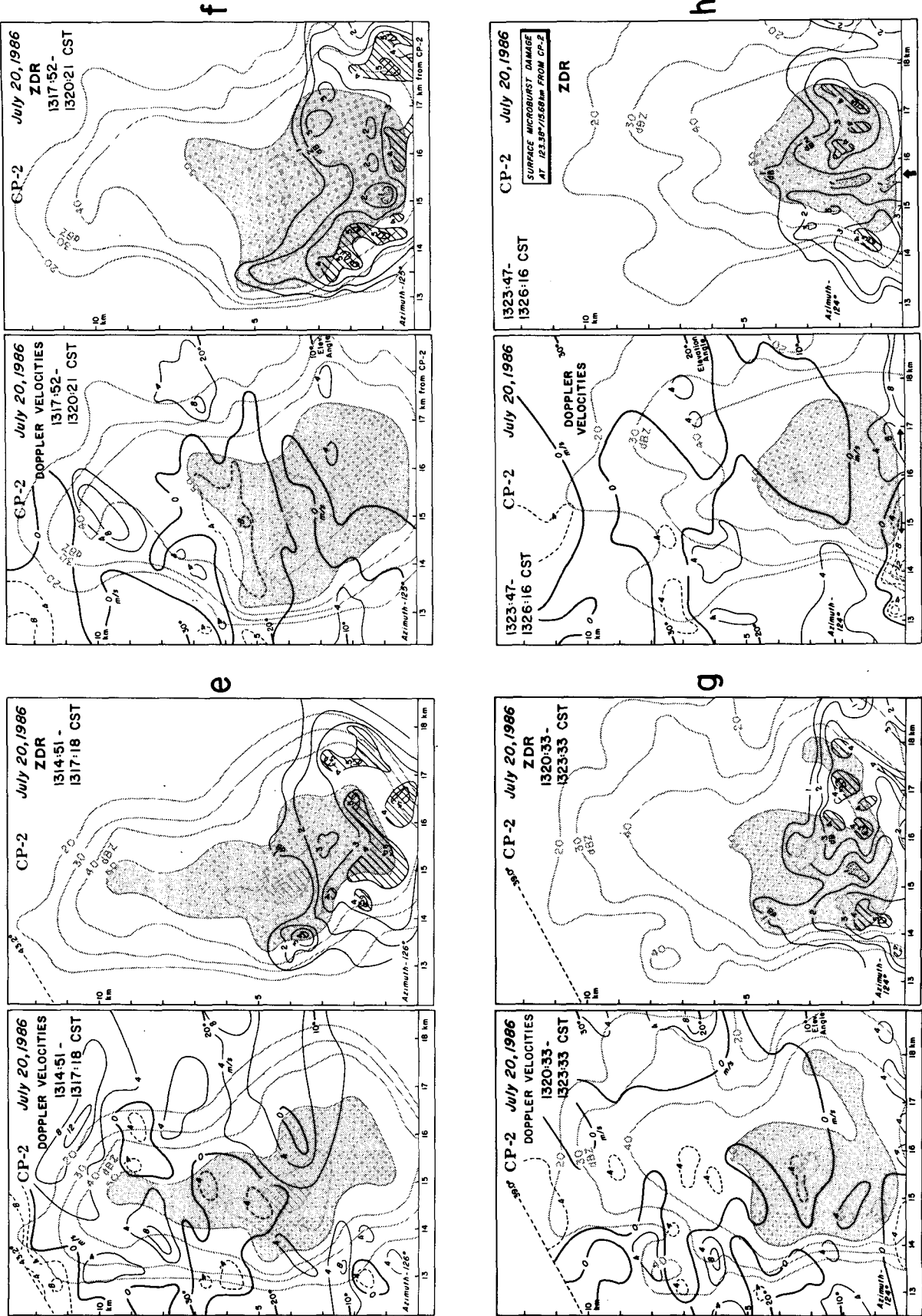


FIG. 10. (Continued)

is called the  $Z_{DR}$  hail signature by Bringi et al. (1986b) and Aydin et al. (1986). Graupel that is assumed to be conical in shape does not generally exhibit complex tumbling motions; therefore, their  $Z_{DR}$  is in the range 0–0.5 dB (see Bringi et al. 1986a). However, as the conical graupel melt to form raindrops the  $Z_{DR}$  signature increases uniformly with decreasing height below the 0°C level from  $\sim 0$  dB to positive values (2–4 dB). Thus the vertical structure of  $Z_{DR}$  below the 0°C level gives an excellent indication of the onset and progression of melting ice into raindrops (see also Hall et al. 1984).

In this paper the reflectivity,  $Z_{DR}$  and mean Doppler velocity fields from the CP-2 radar have been analyzed jointly to sense remotely the microphysical evolution of the 20 July microburst. The full multiparameter radar analysis for this case has been performed by Tuttle, Bringi, Orville, and Kopp (personal communication, 1987) including a comparison with two-dimensional model simulations. These results will be published shortly.

Using the multiparameter information from the CP-2 radar during MIST (see Fig. 1 for the radar location), RHI cross sections of radar reflectivity, single Doppler velocity, and  $Z_{DR}$  were constructed through the 20 July storm (Fig. 10). Velocity measurements combined with reflectivity have been used by Roberts and Wilson (1986, 1987) for identifying precursors for wind-shear warnings; however, this is the first time that  $Z_{DR}$  measurements have been examined for a microburst-producing storm.

In Fig. 10a (a time corresponding to Fig. 7a) there are two small cells apparent with the larger cell having reflectivities exceeding 40 dBZ. Based on Fig. 9, the  $Z_{DR}$  values at this time reveal that both of these cells are composed entirely of raindrops (maximum  $Z_{DR} > 4$  dB) apparently growing via the “warm” rain process. Single Doppler velocity measurements, suggest (as indicated by the dashed black arrow) a strong inflow and updraft into the storm. It is amazing that in just a few minutes the 1306:18–1308:49 CST cross section exhibits tremendous growth of the larger cell owing to the updraft support. There are still indications of strong inflow into the storm and maximum  $Z_{DR}$  values have increased to 5 dB. This liquid precipitation above 5 km are supercooled raindrops based on the sounding in Fig. 4. However, upon close examination of the reflectivity and  $Z_{DR}$  fields in Fig. 10b, it becomes apparent that a large fraction of the 60 dBZ core has relatively low  $Z_{DR}$  values, an indication that frozen precipitation has developed. In fact the top portions of the cloud (20–40 dBZ) have  $Z_{DR}$  values between 0–1 dB. Again in reference to Fig. 7b, it is interesting that the 20 July storm does not visually appear to be glaciated even though the multiparameter information indicates that this has indeed taken place. One explanation is the difference between a cloud photo revealing the visual appearance of the cloud droplets and the radar measurements from rain and ice particles. The cloud drop-

lets are not radar detectable and could be supercooled water and thus appear to an observer as a water cloud even though frozen precipitation exists within its boundaries.

By 1309:00–1311:32 CST (Fig. 10c) the cell has increased in intensity with a substantial area of 60 dBZ still supported by strong velocities away from the radar leading into the main precipitation core. More importantly, the  $Z_{DR}$  measurements suggest that this core is almost entirely composed of ice. Indeed, the values of radar reflectivity and  $Z_{DR}$  within the main precipitation core satisfy the criteria for hail as discussed by Aydin et al. (1986).

The descent of the precipitation core is evident in Fig. 10d. The strong inflow is no longer present in the single-Doppler velocity measurements. It should also be noted that there are no indications of a convergent velocity field above the precipitation core, a common precursor of a developing downdraft discussed by Roberts and Wilson (1986, 1987). The  $Z_{DR}$  values reveal an extensive area of ice above 5 km with large raindrops below this level. This radar observed melting level agrees well with the Redstone sounding shown in Fig. 4. By 1314:51–1317:18 CST (Fig. 10e), the main precipitation core has descended  $\sim 4$  km and has resulted in a “melting-level depression” (Bringi et al. 1986a) in the  $Z_{DR}$  field at  $\sim 14.5$  km from the radar. At a height between 8–9 km, a convergent velocity field is now apparent above the precipitation core.

In Fig. 10f, g, the single Doppler velocity field is not informative except at the surface in Fig. 10g illustrating the beginning of a divergent couplet centered at  $\sim 15.5$  km associated with the developing microburst winds. At the same time, the  $Z_{DR}$  field shows a remarkable evolution of the melting-level depression. A very narrow shaft ( $< 1$  km wide) of low  $Z_{DR}$  ( $\sim 0$  dB) is descending to the surface with the microburst. It should be mentioned that the RHI sections shown in Fig. 10 are reconstructed from PPI scans; however, all values for each individual radar gate (200 m in length) have been plotted for each radial (average elevation angle step  $\sim 1.5^\circ$ ) before contouring. In Fig. 10g, it is noteworthy that the shaft of low  $Z_{DR}$  does not appear to correlate with the pockets of high radar reflectivity.

At 1323:47–1326:16 CST (Fig. 10h), the microburst winds at the surface are clearly indicated by the Doppler velocities. In addition, a well-defined “ $Z_{DR}$ -Hole” is evident in the multiparameter field with several 0 dB values within the 1 dB isopleth. The center of the microburst damage at the surface as determined from ground and aerial survey is  $123.38^\circ$  azimuth at 15.68 km from CP-2. This is well-correlated with the center of the  $Z_{DR}$ -Hole in Fig. 10h. This figure is an excellent example of the microphysical variations across a fairly uniform reflectivity field. Although there is a large core of 50 dBZ and greater values, part of this precipitation is large raindrops while the  $Z_{DR}$ -Hole is composed of melting hail. The values of radar reflectivity and  $Z_{DR}$  again satisfy the criteria for the presence of hail as dis-

cussed by Aydin et al. (1986). Further confirmation of the microphysical characteristics of the  $Z_{DR}$ -Hole was provided by a chase team, which reported pea-size hail at the surface. Note in Fig. 10h that the 60 dBZ core does not correlate with the location of the  $Z_{DR}$ -Hole; this is similar to earlier analyses. This result is consistent with findings by Burrows and Osborne (1986) that precipitation loading was of significance in the formation of microbursts but may not have been sufficient in itself. They report finding strong downdrafts within the 50 dBZ contour; however, strong downdrafts were not everywhere within the 50 dBZ contour.

## 5. Summary and discussion

An attempt was made to use the radar observations of the 20 July storm to determine the operational capabilities of this remote sensing platform. In particular, special attention was placed on the evolution of the dual-polarization fields during the microburst event. The identification of a  $Z_{DR}$ -Hole accompanying the microburst on 20 July 1986 may have important implications for wind-shear detection. Although dual polarization techniques are not presently planned for operational radars, they may be useful in locating a possible strong downdraft by identifying a localized cold core of water-coated ice. It should be emphasized that melting-level depressions have been documented before (e.g., Bringi et al. 1986a); however, the extreme narrowness (<1 km wide) in the horizontal dimensions of the  $Z_{DR}$ -Hole is a unique observation (compare Fig. 10 with Figs. 8b and 10b from Bringi et al. 1986b). Although the small horizontal dimension of the  $Z_{DR}$ -Hole is surprising, the observation of melting hail within a vigorous downdraft is not. Knupp (1985) and Srivastava (1987) have already shown that melting and evaporation of precipitation are primary mechanisms

for driving an intense downdraft. The sounding in Fig. 4 supports strong evaporative cooling below cloud base.

Figure 11 is a schematic model illustrating the probable evolution of the microphysics within the 20 July storm based on the observations of the multiparameter radar. In order to make a further assessment of the reliability of the  $Z_{DR}$ -Hole for microburst detection, two other cases on 13 and 16 July are presented in Fig. 12. These two storms produced differential microburst outflows of 14 and 17 m s<sup>-1</sup>, respectively, and would be classified as moderate to weak wind shear. The soundings for these two days are remarkably similar to Fig. 4 suggesting that the environmental conditions for all three storms are the same and, therefore, direct comparisons can be made. In Fig. 12 the black arrows denote the centers of the microburst outflows which are located directly beneath narrow  $Z_{DR}$ -Holes (<1 km) in both cases. However, unlike the 20 July storm the minimum  $Z_{DR}$  values are between 1 and 2 dB which implies a core of rain mixed with melting hail. It is interesting to speculate whether a relationship between the minimum  $Z_{DR}$  values of the hole and the microburst outflow speeds exists. Furthermore, similar to the 20 July case, both storms in Fig. 12 illustrate that the highest reflectivity values may not correspond to the location of the downdraft. Recently, Jim Wilson (personal communication) has examined another microburst producing storm on 24 June during MIST displaying the same characteristics as shown in Fig. 10. In that case, the  $Z_{DR}$ -Hole was only a few radar gates in length (<1 km) and minimum differential reflectivity values were 0 dB.

The promise of detecting microbursts with  $Z_{DR}$ -Doppler radars should be considered before operational radars are deployed. One of the controversial issues concerning the use of single-Doppler radar observations is how to deal with the asymmetries in the microburst

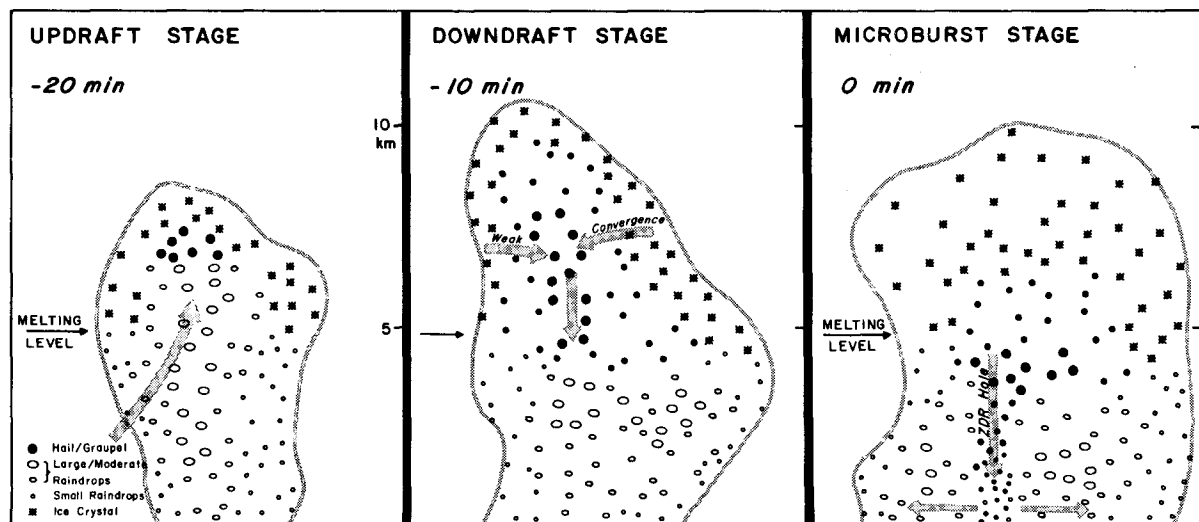


FIG. 11. Schematic model of the microphysical evolution of the 20 July storm.

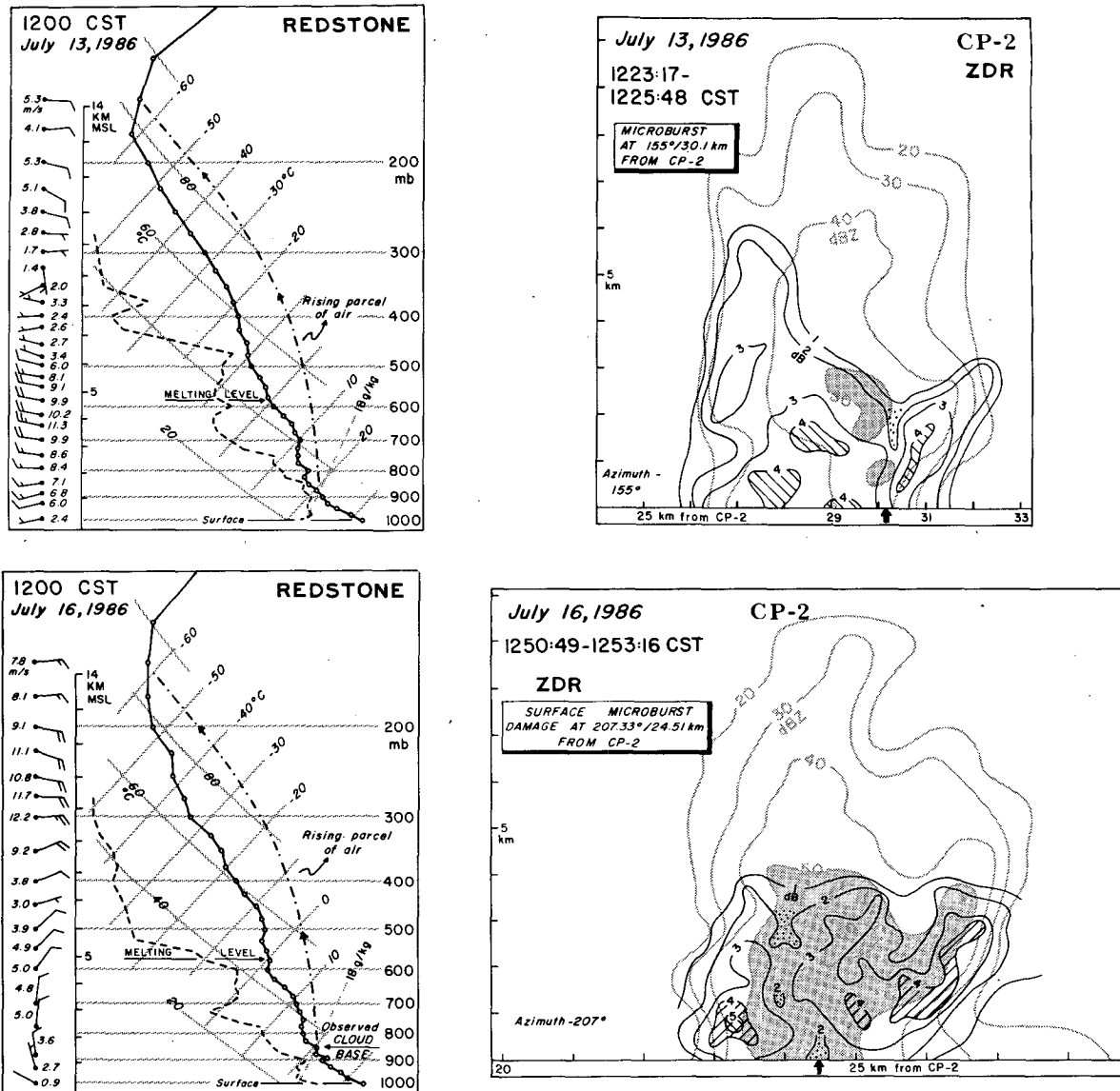


FIG. 12. Environmental soundings and radar reflectivity and  $Z_{DR}$  measurements for two microburst-producing storms on 13 and 16 July 1986. The black arrows denote the location of the center of the microburst at the surface.

outflows (Eilts and Doviak 1987) resulting in a dilemma as to whether an off- or on-airport site for the radar is preferable (Wilson et al. 1984). Since the  $Z_{DR}$ -Hole is hypothesized to be axisymmetric, there would be no preferred viewing angle. Furthermore, the descent of the hole would be an excellent precursor when combined with other criteria established by Roberts and Wilson (1986, 1987) for microburst warnings. By carefully including important detection algorithms it is believed that a reliable Doppler radar system can be developed to protect airports from weather-related hazards.

*Acknowledgments.* The authors wish to express their appreciation to the other MIST principal investigators, Professors T. T. Fujita and Gregory S. Forbes. The

authors also wish to thank James Wilson of NCAR for his tireless effort in providing us with the best possible data, Kevin Knupp of the University of Alabama at Huntsville for providing the 20 July cloud photos, and Greg Forbes of The Pennsylvania State University for providing the damage survey. The FLOWS mesonet data in Fig. 6 used in this paper were provided by MIT Lincoln Laboratory under sponsorship from the Federal Aviation Administration. This research was sponsored by the National Science Foundation (NSF) Grant ATM 87 03143 to UCLA and by NSF Grant ATM 85 19369 to Colorado State University.

REFERENCES

Anderson, R. K., J. P. Ashman, F. Bittner, G. R. Farr, E. W. Ferguson, V. J. Oliver and A. H. Smith, 1972: Applications of meteoro-

- logical satellite data in analysis and forecasting. ESSA Tech. Rep. NESC-51, Washington, D.C., 260 pp [NTIS AD-740-017].
- Aydin, K., T. A. Seliga and V. Balaji, 1986: Remote sensing of hail with a dual linear polarization radar. *J. Climate Appl. Meteor.*, **25**, 1475-1484.
- Bringi, V. N., T. A. Seliga and K. Aydin, 1984: Hail detection with a differential reflectivity radar. *Science*, **225**, 1145-1147.
- , R. M. Rasmussen and J. Vivekanandan, 1986a: Multiparameter radar measurements in Colorado convective storms. Part I: Graupel melting studies. *J. Atmos. Sci.*, **43**, 2545-2562.
- , J. Vivekanandan and J. D. Tuttle, 1986b: Multiparameter radar measurements in Colorado convective storms. Part II: Hail detection studies. *J. Atmos. Sci.*, **43**, 2564-2577.
- Brown, J. M., K. R. Knupp and F. Caracena, 1982: Destructive winds from shallow, high-based cumulonimbi. *Preprints, 12th Conf. Severe Local Storms*, San Antonio, Amer. Meteor. Soc., 45 Beacon St., Boston MA 02108, 272-275.
- Burrows, D. A., and L. F. Osborne, 1986: Precipitation loading in wet microbursts. *Preprints, 23rd Conf. on Radar Meteorology*, Snowmass, Amer. Meteor. Soc., 45 Beacon St., Boston MA 02108, J97-J100.
- Byers, H. R., and R. R. Braham, Jr., 1949: *The Thunderstorm*. U.S. Govt. Printing Office, Washington, D.C., 287 pp.
- Campbell, S. D., 1986: Microburst recognition: An expert system approach. *Preprints, 23rd Conf. on Radar Meteorology*, Snowmass, Amer. Meteor. Soc., R26-R29.
- Caracena, F., and M. Maier, 1987: Analysis of a microburst in the FACE meteorological mesonet network in southern Florida. *Mon. Wea. Rev.*, **115**, 969-985.
- , J. McCarthy and J. Flueck, 1983: Forecasting the likelihood of microbursts along the front range of Colorado. *Preprints, 13th Conf. on Severe Local Storms*, Tulsa, Amer. Meteor. Soc., 45 Beacon St., Boston MA 02108, 261-264.
- Dodge, J., J. Arnold, G. Wilson, J. Evans and T. T. Fujita, 1986: The Cooperative Huntsville Meteorological Experiment (COH-MEX). *Bull. Amer. Meteor. Soc.*, **67**, 417-419.
- Eilts, M. D., 1987: Low Altitude wind shear detection with Doppler radar. *J. Climate Appl. Meteor.*, **26**, 96-106.
- , and R. J. Doviak, 1987: Oklahoma downbursts and their asymmetry. *J. Climate Appl. Meteor.*, **26**, 69-78.
- Evans, J. E., and D. Johnson, 1984: The FAA transportable Doppler weather radar. *Preprints, 22nd Conf. on Radar Meteorology*, Zurich, Amer. Meteor. Soc., 45 Beacon St., Boston MA 02108, 246-250.
- Fujita, T. T., 1978: Manual of downburst identification for Project NIMROD. SMRP. Res. Pap. No. 156, The University of Chicago, NTIS PB 286048, 104 pp.
- , 1979: Objectives, operation, and results of Project NIMROD. *Preprints, 11th Conf. on Severe Local Storms*, Kansas City, Amer. Meteor. Soc., Boston MA 02108, 259-266.
- , 1981: Tornadoes and downbursts in the context of generalized planetary scales. *J. Atmos. Sci.*, **38**, 1511-1534.
- , 1985: The downburst. SMRP Res. Paper No. 210, NTIS PB-85-148880. 122 pp.
- , 1986: DFW microburst. SMRP Res. Paper No. 217, NTIS PB 86-131 638, 154 pp.
- , and F. Caracena, 1977: An analysis of three weather-related aircraft accidents. *Bull. Amer. Meteor. Soc.*, **58**, 1164-1181.
- , and R. M. Wakimoto, 1981a: Five scales of airflow associated with a series of downbursts on 16 July 1980. *Mon. Wea. Rev.*, **109**, 1438-1456.
- , D. J. Stiegler, and R. M. Wakimoto, 1979: The effects of side lobes upon measured Doppler velocities in weak echo regions. *Preprints, 11th Conf. on Severe Local Storms*, Kansas City, Amer. Meteor. Soc., 45 Beacon St., Boston MA, 02108. 509-514.
- Hall, M. P. M., J. W. F. Goddard and S. M. Cherry, 1984: Identification of hydrometeors and other targets by dual-polarization radar. *Radio Sci.*, **19**, 132-140.
- , S. M. Cherry, J. W. F. Goddard and G. R. Kennedy, 1980: Raindrop sizes, and rainfall rate measured by dual-polarization radar. *Nature*, **285**, 195-198.
- Kamburova, P. L., and F. H. Ludlam, 1966: Rainfall evaporation in thunderstorm downdrafts. *Quart. J. Roy. Meteor. Soc.*, **92**, 510-518.
- Kessinger, C. J., R. D. Roberts and K. L. Elmore, 1986: A summary of microburst characteristics from low-reflectivity storms. *Preprints, 23rd Conf. on Radar Meteorology*, Snowmass, Amer. Meteor. Soc., 45 Beacon St., Boston MA 02108, J105-J108.
- Knupp, K. R., 1985: Precipitating convective cloud downdraft structure: A synthesis of observations and modeling. Atmospheric Science Paper No. 387, Dept. of Atmospheric Sciences, Colorado State University, Fort Collins, CO 80523, 242 pp.
- Krumm, W. R., 1954: On the cause of downdrafts from dry thunderstorms over the Plateau Area of the United States. *Bull. Amer. Meteor. Soc.*, **35**, 122-125.
- McCarthy, J., and R. Serafin, 1984: The microburst: Hazard to aviation. *Weatherwise*, **37**, 120-127.
- , J. W. Wilson and T. T. Fujita, 1982: The Joint Airport Weather Studies Project. *Bull. Amer. Meteor. Soc.*, **63**, 15-22.
- , J. W. Wilson and M. R. Hjelmfelt, 1986: Operational wind shear detection and warning: The "CLAWS" experience at Denver and future objectives. *Preprints, 23rd Conf. on Radar Meteorology*, Snowmass, Amer. Meteor. Soc., 45 Beacon St., Boston MA, 02108, R18-R21.
- National Transportation Safety Board, 1983: Aircraft accident report: Pan American World Airways, Inc., Clipper 759, Boeing 727-235, N4737, New Orleans International Airport, Kenner, Louisiana, July 9, 1982. 113 pp. [NTIS PB 83-910402.]
- Pruppacher, H. R., and J. D. Klett, 1978: *Microphysics of clouds and precipitation*. D. Reidel, 714 pp.
- Roberts, R. D., and J. W. Wilson, 1986: Nowcasting microbursts events using single Doppler radar data. *Preprints, 23rd Conf. on Radar Meteorology*, Snowmass, Amer. Meteor. Soc., 45 Beacon St., Boston MA 02108. R14-R17.
- , and —, 1987: Nowcasting microbursts using Doppler radar in a forecasting-computer environment. *Proceedings, Symp. on Mesoscale Analysis and Forecasting Incorporating Nowcasting*, Vancouver, European Space Agency, ESA SP-282, 43-48.
- Seliga, T. A., and V. N. Bringi, 1976: Potential use of radar differential reflectivity measurements at orthogonal polarizations for measuring precipitation. *J. Appl. Meteor.*, **15**, 69-76.
- Srivastava, R. C., 1985: A simple model of evaporatively driven downdraft: Application to microburst downdraft. *J. Atmos. Sci.*, **42**, 1004-1023.
- , 1987: A model of intense downdrafts driven by melting and evaporation of precipitation. *J. Atmos. Sci.*, **44**, 1752-1773.
- Wakimoto, R. M., 1983: The West Bend, Wisconsin Storm of 4 April 1981: A problem in operational meteorology. *J. Climate Appl. Meteor.*, **22**, 181-189.
- , 1985: Forecasting dry microburst activity over the High Plains. *Mon. Wea. Rev.*, **113**, 1131-1143.
- Wilson, J. W., and W. E. Schreiber, 1986: Initiation of convective storms at radar-observed boundary-layer convergence lines. *Mon. Wea. Rev.*, **114**, 2516-2536.
- , R. D. Roberts, C. Kessinger and J. McCarthy, 1984: Microburst wind structure and evaluation of Doppler radar for airport wind shear detection. *J. Climate Appl. Meteor.*, **23**, 898-914.
- Wolfson, M., 1987: The FLOWS automatic weather station network. *Preprints, Sixth Symp. on Meteorological Observations & Instrumentation*, New Orleans, Amer. Meteor. Soc., 45 Beacon St., Boston, MA 02108, 294-299.